Pergamon

Int. J. Multiphase Flow Vol. 24, No. 3, pp. 359–386, 1998

Printed in Great Britain
PII: S0301-9322(97)00054-2
0301-9322/98 $19.00 + 0.00

THE EFFECT OF PARTICLES ON WALL TURBULENCE

D. KAFTORI†, G. HETSRONI‡ and S. BANERJEE
Dept. of Chemical and Nuclear Engineering, University of California at Santa Barbara, Santa Barbara, CA 93106, U.S.A.

(Received 1 March 1997; in revised form 23 July 1997)

Abstract—The effect of a dilute suspension, of near neutral-density particles, on the wall turbulence in a horizontal channel was investigated by means of a laser Doppler anemomentry and flow visualization.

We found that the particles increase the period between bursts. However, due to the mixing effect of the particles and effects similar to a rough wall, the overall Reynolds stress increases somewhat near the wall. Furthermore, because of increased Reynolds stress levels within the bursts, the fraction of the Reynolds stress in the bursts remains at about the same value (~85%) as for flows without particles. Quadrant analysis of the Reynolds stress data indicates that particles increase sweep activity near the wall, i.e. in the region ≤10 wall units. All this results in increased wall normal velocity fluctuations in the viscous sublayer that may significantly impact heat and mass transfer rates. Estimates based on the data indicate an increase of ~18% in heat transfer rates with only 5% increase in wall friction. © 1998 Published by Elsevier Science Ltd. All rights reserved

Key Words: two-phase flow, particles–turbulence interaction, turbulence modulation

1. INTRODUCTION

Recent studies show that suspended particles may substantially affect turbulence parameters and transport properties. For example, particles can enhance or suppress turbulence, depending on their size and concentration (see Gore and Crowe 1989; Hetsroni 1989 for a review), or they may increase the rate of wall heat transfer (e.g. Zisselmar and Molerus 1979; Hetsroni and Rozenblit 1994). These effects must be taken into account when modeling two-phase flows and it cannot be assumed that the turbulence properties of the two-phase mixture are the same as those of the pure fluid. Also, particles may tend to agglomerate in some regions, leading to high local concentrations, even when the overall concentration is low. This has been found in homogeneous, isotropic turbulence (e.g. Squires and Eaton 1991; Wang and Maxey 1993), and in shear flow turbulence (e.g. Grass 1982; Lázaro and Lasheras 1989; Rashidi *et al.* 1990; Pedinotti *et al.* 1993; Kaftori *et al.* 1995a,b; Pan and Banerjee 1996). This phenomenon may lead to enhanced local effects and should also be considered when modeling dilute dispersed flows.

The effects of particles are apparent in wall turbulence, which contains large scale persistent structures, as well as in regions far from the boundary, where the turbulence is more homogeneous. Away from the wall, small particles generally suppress turbulence while large ones enhance it (e.g. Tsuji *et al.* 1984; Sun and Faeth 1986; Shuen *et al.* 1985). The terms 'large' and 'small' are used here in the sense of being relative to the length scales of turbulence in the continuous phase. Precise criteria for the scales involved in, and the conditions for, transition from suppression to enhancement are yet to be determined. One suggestion, proposed by Gore and Crowe (1989) based on some experimental data, is that if the ratio of particle diameter to the size of the energy containing eddies is greater than about 0.1, then particles increase turbulence intensity. When the ratio is smaller than 0.1, particles suppress turbulence.

The mechanisms by which particles modify turbulence are also not clear. Turbulence enhancement is believed to be the result of two processes. One is the crossing trajectory effect (e.g. Mei *et al.* 1991) where particles, due to their high inertia, do not follow the fluid motion and cross

†Present address: Silver Arrow, 10 Roujansky St., Rishon-Lezion 75706, Israel.
‡Permanent address: Mechanical Engineering Dept., Technion—Israel Institute of Technology, Haifa 32000, Israel.

from one eddy to another, in the process transferring momentum and causing mixing. The other mechanism is vortex shedding behind particles. Hetsroni (1989) suggested that when the particle Reynolds number is greater than 400, the condition at which vortex shedding begins (Achenbach 1974), turbulence will be enhanced.

Several authors suggest that turbulence suppression may be due to an increase in apparent viscosity due to the particles (e.g. Ishii 1977; Leighton and Acrivos 1986; Lee and Börner 1987). Another suppression mechanism may be density stratification, suggested by Smith and McLean (1977). They showed that if there is a particle concentration gradient across the flow, then there exists a density gradient which produces stable stratification, and damps turbulence.

In the wall region, turbulence is dominated by large scale persistent structures. To date, the nature of these structures, i.e. high- and low-speed regions, quasi-streamwise vortices, ejections and sweeps, is not clearly determined and there is no consensus as to the relationships between them. However, the prevailing notion is that they are related to some form of large scale streamwise vortices (e.g. Robinson 1991; Brooke and Hanratty 1993; Bernard *et al.* 1993). The vortices may be expanding in a shallow angle in the direction of flow, forming a funnel shape (Kaftori *et al.* 1994). Regardless of their exact nature, it appears that these vortices significantly affect particle behavior in the boundary layer (Yung *et al.* 1989; Sumer and Oguz 1978; Kaftori *et al.* 1995a,b).

Close to the wall, particles exhibit a tendency to preferentially accumulate in certain regions. For example, heavier-than-fluid particles which settle to the wall in horizontal flow tend to migrate into the low-speed regions, possibly because they are thrown out of the quasi-streamwise vortices mentioned earlier. This was found both experimentally and in direct numerical simulations in a number of studies. However, the tendency to accumulate in these regions depends on particle size and time constant (defined below), where particles with a non-dimensional time constant of approximately 3 tend to agglomerate more than larger or smaller particles. These findings imply an interaction between the particles and the persistent turbulence structures, which results in particle segregation when they have time constants in the appropriate range. Also, when the particles are small enough, they may get trapped in the viscous layer, where they are relatively immune to resuspension mechanisms. This was found by Brooke *et al.* (1992) using numerical simulation of flow in a vertical channel. In horizontal flow the effect is further enhanced due to gravitational forces. Kaftori *et al.* (1995b) also showed that particle concentrations in the wall structures are higher than elsewhere, resulting in regions with distinct flux gradients corresponding to the various main regions of the turbulent boundary layer, i.e. the viscous, log-law, and wake regions.

The high local concentration in the low-speed regions may be significant for the understanding of how particles enhance transport processes at the wall. In the low-speed regions, the shear rate, and consequently the heat transfer coefficient, are low compared with the high-speed, and high shear, regions. The higher concentration of particles in the low-speed regions may induce mixing locally, thus potentially enhancing the heat transfer rate in these regions. The enhancement is probably related to an increase of the low frequency wall normal velocity fluctuations which have been shown to control transport processes at the boundary (Campbell and Hanratty 1983).

Rashidi *et al.* (1990) were the first to conduct experiments aimed specifically at determining the effects that particles may have on wall turbulence. Their experiments were confined to only one Reynolds number, i.e. 5000, based on flow depth and average velocity, and with slightly heavier-than-fluid particles. Their observations showed that near the wall particles accumulate in the low-speed streaks, and that small particles increased the average time between wall ejections while large particles reduced it. There was no significant effect on the time between bursts – which they defined as consisting of closely grouped ejections, and sweeps. Thus in some sense the findings related to the activity level within bursts. Large particles, on average, increased the turbulence intensities and Reynolds stress in the core region, while small particles reduced them. The effects were stronger at higher concentrations. Rashidi *et al.* could not make observations close to the wall because of their measurement technique using microbubble tracers.

The current work is part of an experimental investigation of particle–turbulence interaction, using laser Doppler anemometry (LDA) and flow visualization. The goal was to investigate the

interaction between particles and turbulence in the boundary layer, and in particular, near the wall. An objective conditional-sampling method for identifying the wall structures (the 'active' periods) is applied. In the first parts of this work (Kaftori *et al.* 1995a,b) the motion, entrainment and deposition of particles under the influence of the wall structures were examined, and it was found that these structures dominate most aspects of particle behavior. This paper focuses primarily on the effect of particles on the turbulence itself. In particular, we are interested in the effects that particles may have on the wall normal velocity fluctuations since these primarily affect heat and mass transfer (Campbell and Hanratty 1983). Thus, while the low mean particle concentration may have only subtle effects on the turbulence overall, they may still markedly affect the near-wall structure and transport rates.

2. EXPERIMENTS AND PROCEDURE

The experimental facility was the flume described in Kaftori *et al.* (1995a). It is a $4.5 \times 0.32 \times 0.1\ m^3$ open channel, equipped with a 2-D LDA system for data acquisition and with flow visualization techniques using oxygen microbubble tracers and high-speed video. The LDA and high-speed video were synchronized so that the LDA data could be compared with the visually observed flow patterns around the probe volume. The solid particles under investigation were of polystyrene with diameters of 100, 275, and 900 μm and specific density 1.05. Average nominal volumetric concentrations (loading) were 1 and 2×10^{-4}. Details about particle size distribution and concentration measurements can be found in Kaftori (1993) and Kaftori *et al.* (1995a).

Table 1. Experimental conditions

Re_h	Particles	Loading $\times 10^{-4}$	U_m (m/s)	h (mm)	ν (m^2/s) $\times 10^{-6}$	u^* (m/s)
4870	none	—	0.125	31.51	0.808	0.0074
4970	none	—	0.128	31.36	0.808	0.0074
5010	none	—	0.113	33.5	0.755	0.0067
4660	100	1.5[a]	0.138	27.35	0.810	0.0085
5120	275	0.56[a]	0.143	28.41	0.793	0.0086
5040	900	0.65	0.128	31.71	0.806	0.0078
5080	900	0.88	0.128	32.01	0.807	0.0076
7110	none	—	0.164	32.67	0.754	0.0090
7890	none	—	0.195	31.86	0.787	0.0106
8460	none	—	0.204	31.36	0.756	0.0111
8090	275	0.8	0.198	32.06	0.785	0.0111
9130	none	—	0.220	32.81	0.791	0.0124
9900	none	—	0.244	32.80	0.808	0.0128
10070	none	—	0.222	34.33	0.757	0.0115
10210	none	—	0.248	33.15	0.805	0.0127
10420	none	—	0.256	32.90	0.808	0.0127
9850	100	1.87	0.244	32.41	0.803	0.0128
9950	100	2.16	0.246	32.6	0.806	0.0129
10300	275	1.15	0.249	32.86	0.794	0.133
9420	275	2.0	0.227	32.81	0.791	0.0123
10160	275	1.9	0.247	32.46	0.789	0.0132
9870	900	1.03	0.244	32.56	0.805	0.0132
10280	900	0.6	0.257	33.05	0.826	0.0132
9870	900	1.95	0.244	32.6	0.806	0.0135
10070	900	2.3	0.249	32.5	0.804	0.0135
14150	none	—	0.296	37.06	0.775	0.015
14020	none	—	0.294	36.86	0.773	0.015
13660	100	1.87	0.313	34.96	0.801	0.016
13930	100	2.16	0.320	35.40	0.813	0.0160
14180	275	0.87	0.322	35.06	0.796	0.0161
14110	275	1.95	0.320	35.11	0.796	0.0160
14340	900	1.09	0.294	37.76	0.773	0.0155
13900	900	1.99	0.295	37.61	0.798	0.0155

[a] Based on mean flow rate of particles, not considering layers of settled particles.

Table 2. Properties of particles

Property	Nominal diameter (μm)	$Re_h \approx 5000$	$Re_h \approx 10{,}000$	$Re_h \approx 14{,}000$
d_p^+	100	1.06	1.61	1.88
	275	3.0	4.5	5.5
	900	8.66	15.2	17.4
τ_p (s)	100	7.3×10^{-4}		
	275	5.5×10^{-3}	The same	The same
	900	6.0×10^{-2}		
τ_p^+	100	0.065	0.15	0.23
	275	0.51	1.21	1.77
	900	4.41	13.58	18.07
τ (s)[a]	Fluid	0.79	0.46	0.42

[a] Determined from experiments.

The LDA system was designed such that velocities of both particles and fluid (i.e. tracer particles) could be measured in real time using the signal amplitude for discrimination, as described in Kaftori *et al.* (1995b).

The experimental conditions and particle characteristics were detailed in Kaftori *et al.* (1995a) (tables 1 and 2, respectively). In table 2, τ is the characteristic time constant of the fluid away from the wall region, and $\tau_p = (1/18\nu)d_p^2(\rho_p/\rho_f)$ is the particle relaxation time, where d is the particle diameter, ν is the kinematic viscosity, ρ is the density, and subscripts p and f denote particle and fluid, respectively. The superscript + in the text denotes units normalized by wall variables (kinematic viscosity and the friction velocity u^*). Experiments were conducted primarily at Reynolds numbers of 5000, 10,000, and 14,000 ($Re_h = U_m h/\nu$ where U_m is the mean velocity, and h is water level).

The balance between particles settled at the bottom of the flume and particles in suspension was a function of shear rate (represented here by a shear Reynolds number: $Re^* = u^* h/\nu$). Higher shear caused more particles to be entrained, and consequently the number density of particles on the bottom was reduced, as shown in figure 1. It should be noted that all the exper-

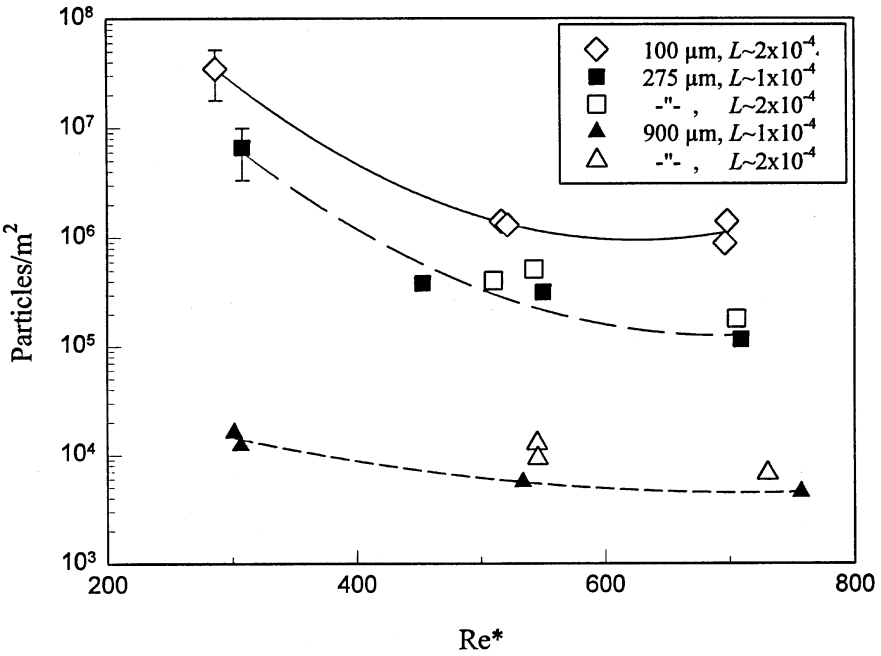

Figure 1. The population density of particles at the wall under various flow conditions. Lines are second order curve fits. The error bars are specific to the conditions where they are shown, where a large uncertainty existed due to the sediment layer. For the other conditions, uncertainties were of the order of the size of the symbols.

iments were performed with approximately the same water depth and therefore the flow Reynolds number (Re_h) is indicative of the wall shear stress.

Near the bottom, heavier-than-fluid particles tended to concentrate in streaks. It appears that the particle streaks coincided with the low-speed regions and that the non-dimensional streak spacing of ~100 wall units was maintained (see also Rashidi *et al.* 1990 and Kaftori *et al.* 1995a).

The concentration distribution throughout the flow was not homogeneous. Even at high Reynolds numbers, when most of the particles were in suspension, the average local concentration near the wall was one to two orders of magnitude higher than in the outer flow regions (Kaftori *et al.* 1995b). The local concentration inside particle streaks was even higher. These local variations may lead to differences in the local effects of particles on the flow, as discussed below. A detailed description of particle behavior, and of the effects of turbulence structures on particle deposition, resuspension, flux, and concentration can be found in Kaftori *et al.* (1995a,b).

3. TURBULENCE MODIFICATION

In this section, the effects of particles on the turbulence characteristics of the flow will be examined. Since the focus is on fluid turbulence, only fluid velocities will be considered. The velocity and concentration data for the particles were discussed in Kaftori *et al.* (1995b).

3.1. *Velocity profile and friction velocity*

For the range of flow conditions of the current work, the friction velocity in particle free flow was a linear function of Reynolds number. This is illustrated in figure 2. The two Reynolds numbers were related by

$$Re^* = 0.0461 Re_h + 64.53. \quad [1]$$

This equation was also accurate in predicting the open channel results of other researchers (e.g. Rashidi and Banerjee 1988; Nezu and Rodi 1986; Grass *et al.* 1991).

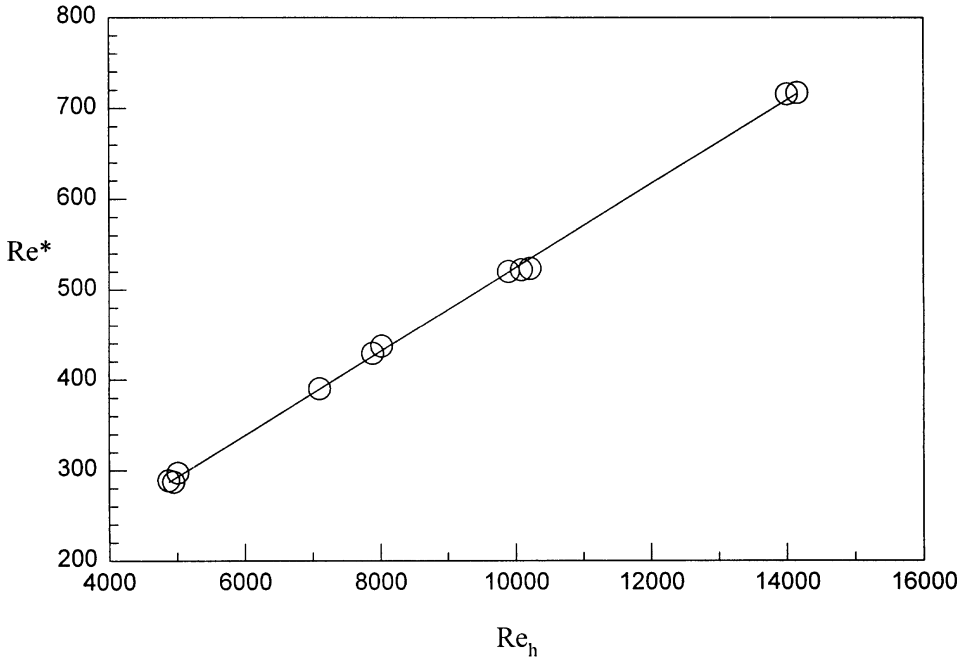

Figure 2. Shear Reynolds number vs. flow Reynolds number. The line is [1].

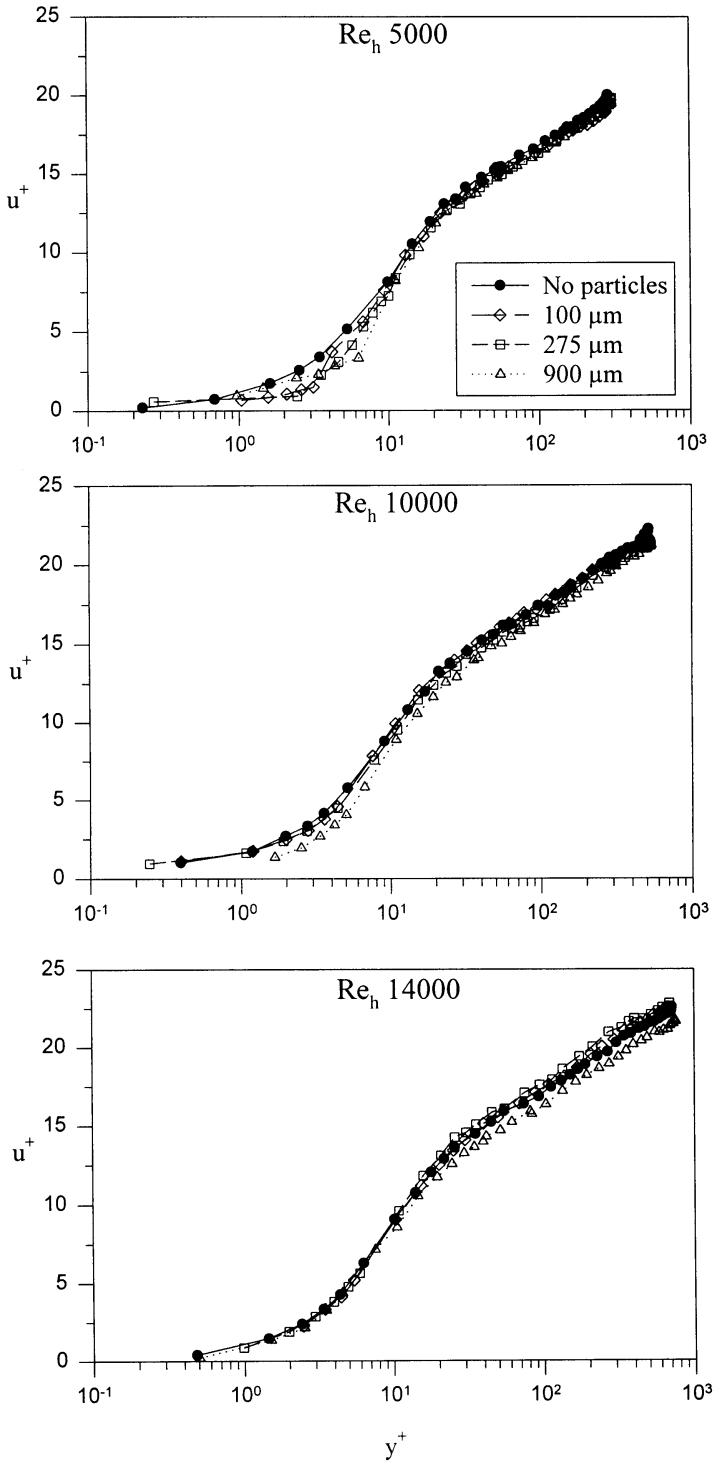

Figure 3. Velocity profiles of some particle-laden and particle-free flows, normalized by wall units.

The effect of particles on the fluid velocity profile is shown in figure 3. Each of the velocity profiles in the figure is normalized by the friction velocity of that particular experiment. The friction velocity was computed using the velocity profile in the viscous layer (Kaftori *et al.*, 1995a). Two phenomena are apparent from the figure. One is that when many particles were settled on the bottom, the velocity profile was shifted towards lower values. This was true with

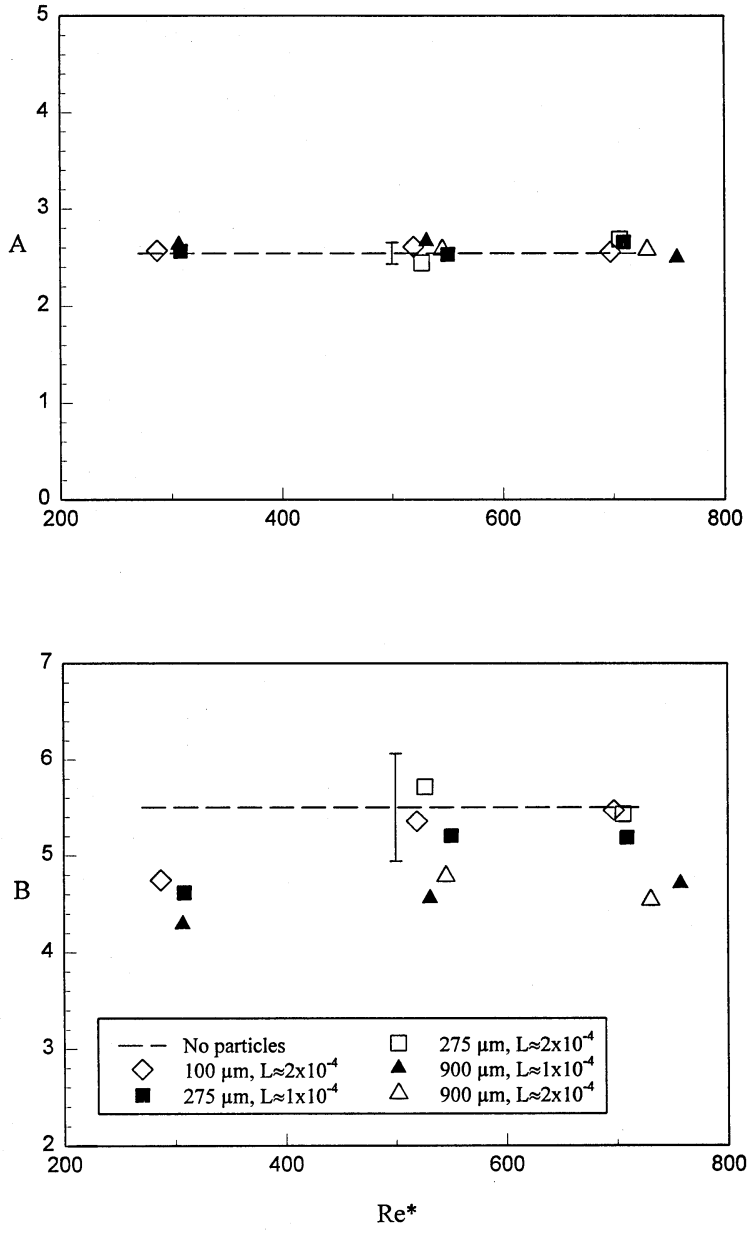

Figure 4. Coefficients of the logarithmic velocity profile: $u^+ = A \ln(y^+) + B$.

all of the particles at $\mathrm{Re}_h = 5000$, and with the 900 μm ones at the higher Reynolds numbers. In other words, the mean velocity was reduced, suggesting that the Reynolds stress should have increased. The second phenomenon is that at $\mathrm{Re}_h \approx 14{,}000$, the 100 and 275 μm particles increased the mean velocity in the outer flow, suggesting that the Reynolds stress there was reduced.

The coefficients of the logarithmic profile:

$$u^+ = A \ln(y^+) + B \qquad [2]$$

were computed from the slope of the curve in the range $30 \leq y^+ \leq 0.2\mathrm{Re}^*$ following Nezu and Rodi (1986). For runs without particles the coefficients were $A = 2.55 \pm 0.11$ and $B = 5.46 \pm 0.56$, where the ($\pm$) indicates a standard deviation. These are in agreement with values found in the literature. For example, Nikuradse reported $A = 2.5$ (Hinze 1975), Schlichting (1979) suggests $B = 5.5$, Nezu and Rodi (1986) found $A = 2.54$, $B = 5.29$, and Lam and Banerjee (1992) found $A = 2.5$, $B = 5.1$.

The effect of particles on the coefficients in [2] is shown in figure 4. The first coefficient was not affected. The second was reduced with large particles, and with all sizes at the low Reynolds number. This is a result of the shifted velocity profiles in figure 3.

The behavior of the particle-laden flow, namely increased wall shear stress and a retardation of the mean velocity, is similar to a flow over a rough wall (Grass 1982; Grass *et al.* 1991). It may, therefore, be worthwhile to examine whether some of the effects of particles on the flow can be expressed in terms of an increased roughness due to the presence of particles at the wall.

Figure 5 depicts the relationship between normalized roughness and wall coverage (a), and between roughness and flow shear rate (b). Wall coverage is the fraction of wall area covered by particles (i.e. $n\pi d_p^2/4$, where n is the number of particles per unit of wall area). The wall roughness is given in terms of a non-dimensional equivalent sand roughness (k_s^+). This parameter represents the size of sand grains, assumed to evenly coat the wall, which would produce the same resistance coefficient as the actual roughness elements, i.e. particles in the present case. The

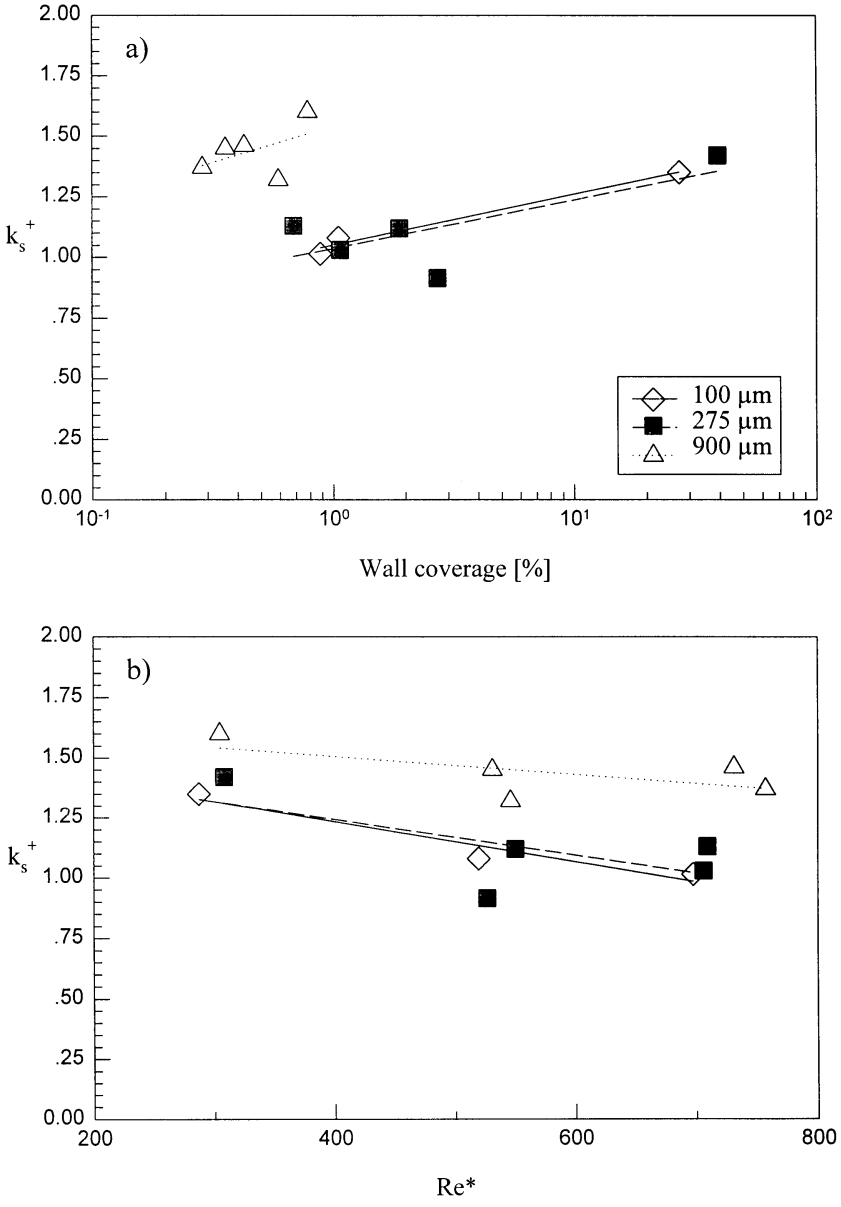

Figure 5. Non-dimensional equivalent sand roughness as a function of wall coverage (a) and of shear rate (b).

equivalent wall roughness was extracted from the slope of the velocity profile following Schlichting (1979).

As can be seen in the figure, k_s^+ was proportional to the wall coverage parameter, and inversely proportional to the shear rate. When more particles were at the wall, the effect was to increase k_s^+. On the other hand, as the shear rate increased, more particles were suspended and fewer remained at the wall (figure 1). This resulted in a reduced k_s^+ value. Also, the larger particles increased the wall roughness more than the two smaller ones. The lines in the figure are linear curve fits, intended to show the general trends in the data. Since the values of the equivalent sand roughness were extracted from the slope of the velocity gradient, they are a third order representation of the effect of particles and scatter is to be expected. Therefore, only the overall effect can be observed, but no accurate values can be extracted here. It should be remembered

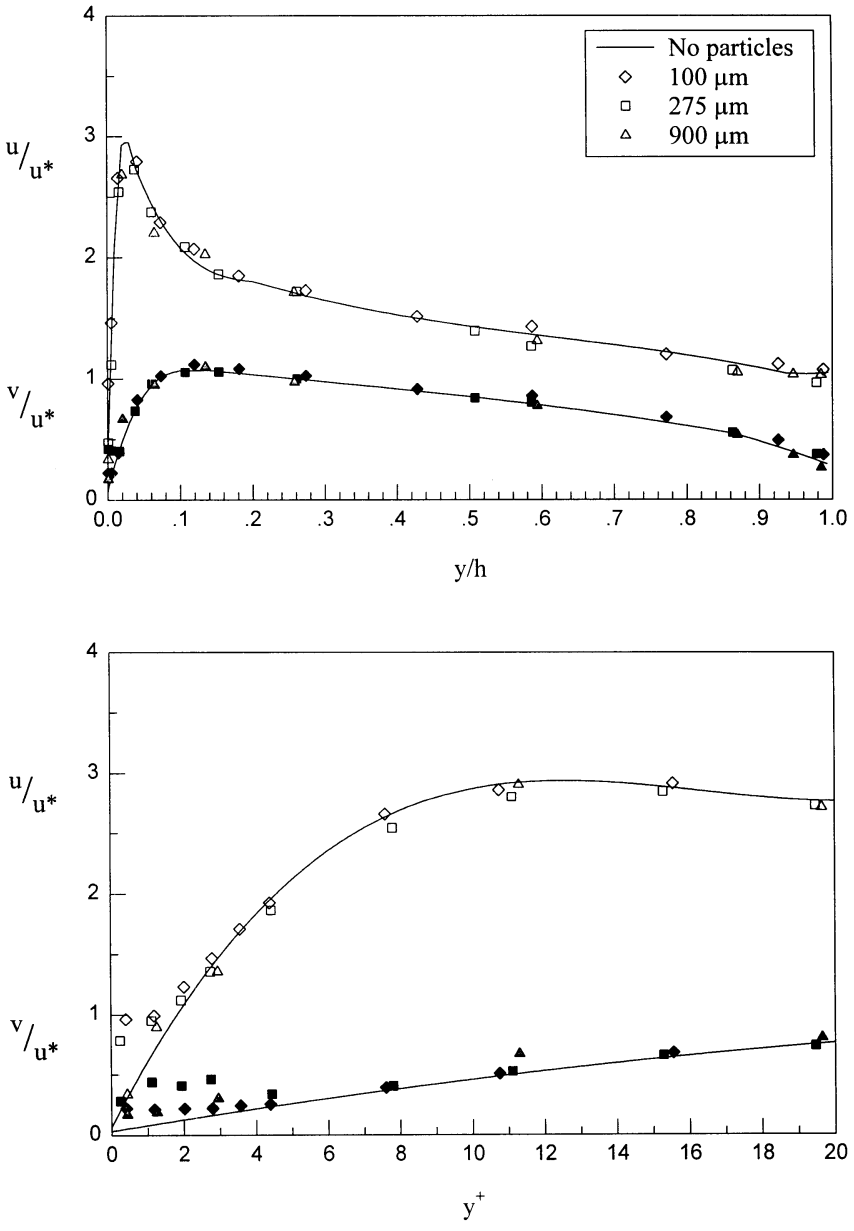

Figure 6. Turbulence intensities with and without particles at $Re_h \approx 10{,}000$. Top – normalized by water depth. Bottom – normalized by wall units. Open symbols are the streamwise component (u) and solid symbols are the wall normal (v).

that in practice, $k_s^+ = 1$ corresponds to a smooth wall. When $k_s^+ > 1$, the shear rate, and accordingly the turbulence intensity and pressure drop, should increase, while $k_s^+ < 1$ represents the case where the turbulence intensity has decreased.

However, in all of the cases examined here, the non-dimensional equivalent sand roughness was small and within the hydraulically smooth regime (i.e. $k_s^+ < 5$, see Schlichting, 1979), so the effect of the particles should be quite small.

3.2. *Turbulence intensities and Reynolds stress*

Sample profiles of turbulence intensity (r.m.s. velocity fluctuations) at $Re_h \approx 10{,}000$ are plotted in figure 6. The corresponding figures of the other flow conditions were very similar and are not shown. It appears that the particles did not affect intensities in the outer flow but did substantially increase them at the wall. The effect is more pronounced in the wall normal component and is limited to the layer of settled particles. Similar observations were reported in the numerical simulations by Pan and Banerjee (1996). The increase in r.m.s. is likely to cause an increase in heat and mass transfer since, as mentioned above, the wall normal velocity fluctuations are the ones responsible for transport processes at the wall.

The Reynolds stress profiles, depicted for a few sample runs in figure 7, do show modifications due to particles. The effects are noticeable away from the wall. The Reynolds stress in the very-near-wall region did not exhibit significant changes and therefore is not plotted in detail. In order to compare the effects of particles to particle-free flows, the Reynolds stresses in figure 7 were normalized by the friction velocities of similar flows without particles, depicted by u_0^*, which were computed by [1]. As can be seen, the Reynolds stresses increased with both particle sizes at $Re_h \approx 5000$. This is consistent with the reduced velocity (figure 3) and increased wall roughness (figure 5). On the other hand, at $Re_h \approx 14{,}000$ the smaller particles reduced the Reynolds stress in the outer flow region. The effect of the 275 μm particles was very similar to that of the 100 μm in figure 7. They were not plotted to avoid obscuring the data in the figure with too many points. This is also consistent with figures 3 and 5.

The modifications of turbulence intensity and Reynolds stress found here are rather small compared, for example, with the works cited by Hetsroni (1989). In all of these works, however, the particles were orders of magnitude heavier than the fluid, and the concentrations much higher than used here. The only comparable work in the literature is that of Rashidi *et al.*

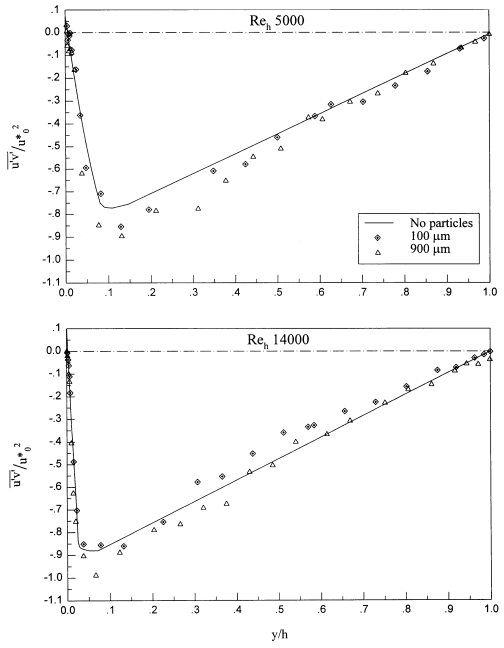

Figure 7. Reynolds stress with and without particles, normalized by the friction velocity of particle-free flow.

(1990), who used the same fluid–particle combination at $Re_h \approx 5000$. They found approximately the same increase in Reynolds stress with large particles. On the other hand, with small particles (120 μm in their work) they noticed a reduction of Reynolds stress which was not observed here at this Reynolds number. However, the reduction was mostly apparent at double the mean concentration used here. In addition, in their work the particles were introduced into the flow in suspension and at a relatively short distance upstream from the measuring point. Therefore, the small particles may not have had time to settle to an equilibrium concentration distribution by the time they reached the measuring point. Consequently, it is likely that the number of particles in suspension at $Re_h \approx 5000$ in their work was closer to the number of particles in suspension at $Re_h \approx 14{,}000$ in the current work, where turbulence suppression was, indeed, apparent.

3.3. *Effects of particles on wall structures*

Since wall turbulence structures exhibit active periods of rotation, acceleration and deceleration, they could be identified and analyzed by conditional sampling of LDA data. In this work, a technique which combines the $u'v'$ level and *tke* level methods was used. The necessary parameters (i.e. threshold levels and a grouping time window) were determined by a systematic optimization algorithm. The technique was developed and tested by using synchronized flow visualization and was then applied to all of the LDA data with consistent results. A detailed description of the technique is given in Appendix A.

The data regarding average quantities, such as time between structures, which are plotted and discussed in this section, combine all similar runs as single points, i.e. the points from all experiments at, say, $Re_h = 4850$–5000 without particles (see table 1) are averaged and represented by one point at the average $Re_h \approx 4925$. Error bars indicate the maximum scatter of the combined no-particles points. This was done in order to clearly distinguish between the various conditions and to identify the trends in the effects of particles.

The addition of particles reduced the number of wall structures in the flow. This can be seen in figure 8 where the average non-dimensional time between structures is plotted for a range of flow conditions at $y^+ \approx 30$. The non-dimensional time is defined as:

$$T^* = \frac{u^{*2}}{\nu} t_g \qquad [3]$$

where t_g is the average time between conditionally sampled groups of events (see Appendix A).

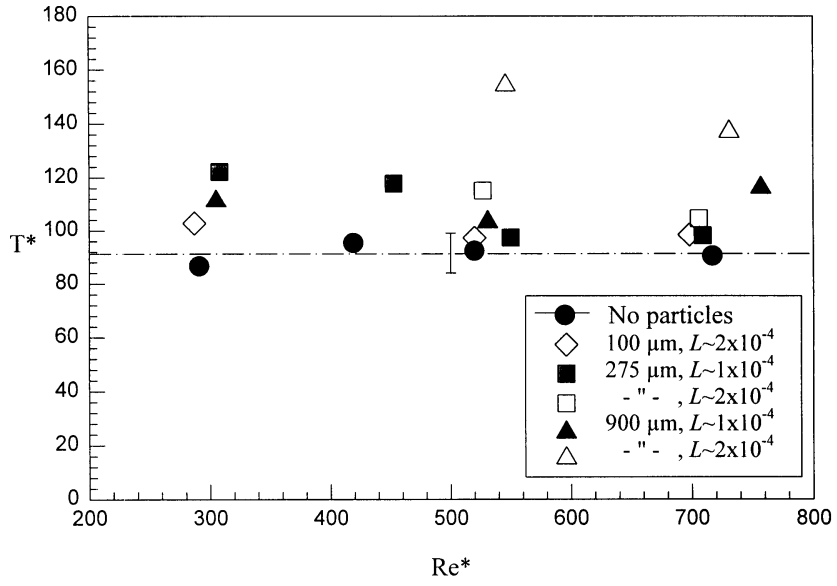

Figure 8. Average non-dimensional time between wall structures as a function of shear rate. Dashed line represents average of all runs without particles. Error bars indicate maximum scatter of particle-free flows.

For flow without particles, the combined average of all runs, regardless of Reynolds number, was approximately 91, which is in agreement with the value of 90 found by Luchik and Tiederman (1987) and 85 found by Rashidi and Banerjee (1990) for the time between bursts. With the introduction of particles, T^* increases significantly – up to 50%, depending on particle size and loading ratio. Thus particles reduce the frequency of occurrence of these structures. In general, for a given Reynolds number and particle size, the effect was stronger when more particles were present.

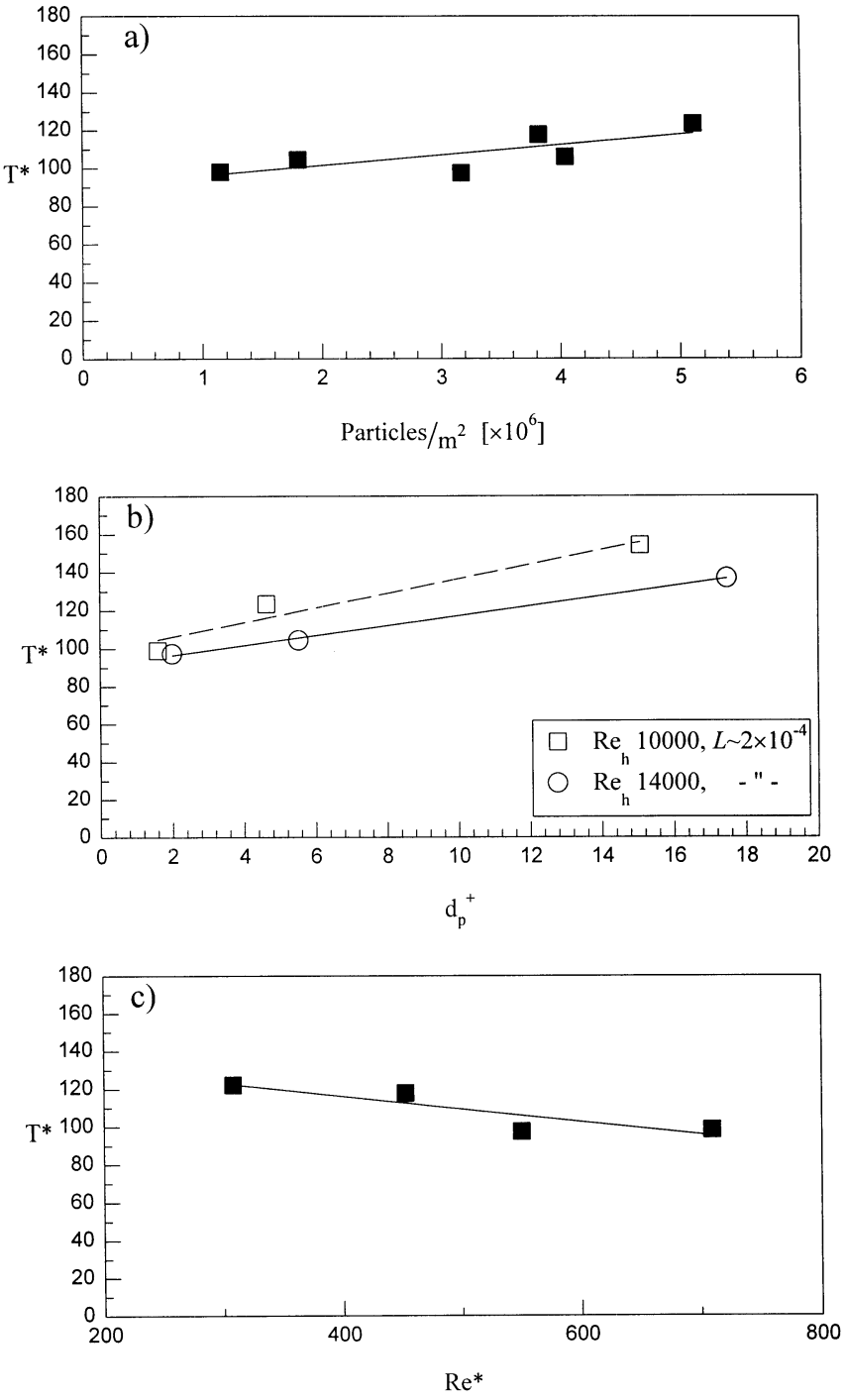

Figure 9. Time between structures: (a) as a function of the particle number density at the wall (with 275 μm particles); (b) as a function of non-dimensional particle size; and (c) as a function of shear Reynolds number for the 275 μm particles at the lower loading ratio.

The reduction in the frequency of wall structures is a result of a number of factors. One is the particle number density near the wall. The more particles of a given size are at the wall, the stronger the reduction in the number of structures. This is shown in figure 9(a). Another factor is the (non-dimensional) particle size. Larger particles increase the time between structures more than small ones [figure 9(b)]. The last factor is the shear rate. As shown in figure 9(c), the effect of particles diminishes as the shear rate is increased. This seems to be counter-intuitive, since as the shear rate increases, the particles become larger relative to the scales of turbulence. The reason for the reverse trend is that at higher shear rates more particles become suspended and the concentration at the wall is reduced (figure 1). This, in turn, lessens the effect on the time between structures, as in figure 9(a). The effect of the shear rate is thus a balance between these two factors.

The frequency of wall structures in the presence of particles, divided by the non-dimensional particle size, scales well with the non-dimensional size to the second power. This can be seen in figure 10. Note, however, that D^{+2} in this work is directly proportional to the non-dimensional particle relaxation time because all of the particles were of the same density. This suggests that the frequency is, in fact, dependent on both the size and density of the particles. This must be examined further by using particles of various sizes. In any case, it seems that the time between wall structures in the presence of particles scales with wall variables, as it does in clear fluid.

In spite of the substantial reduction in the frequency of the wall structures, the particles hardly affected the fraction of Reynolds stress or turbulent kinetic energy held in them. As can be seen in figure 11, approximately the same relative amount of Reynolds stress is found in the structures in both particle-laden and particle-free flows. The combined average of all the experiments was approximately 85%. The same was true for the turbulent kinetic energy inside the structures (figure 12), where the combined average of turbulent kinetic energy in them was 68% for both particle-laden and clear fluid.

The quantities found above for the time between structures and the fraction of Reynolds stress held in them compare well with values found in the literature for the time between, and Reynolds stress within, bursts.

Finally, as was mentioned above, particles did not change the appearance of the streaky structures within the wall layer. In general the particles tended to accumulate in the low-speed streaks. However, this tendency depends on particle size and time constant, with medium size particles ($\tau_p^+ \sim 3$) accumulating in streaks more than the larger or smaller ones (see Kaftori *et al.* 1995a).

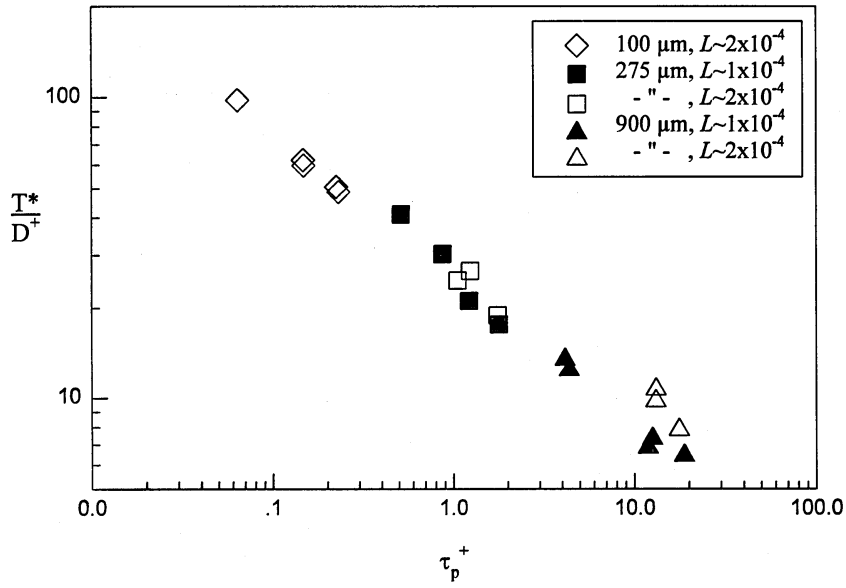

Figure 10. Time between structures as a function of the non-dimensional particle size and relaxation time.

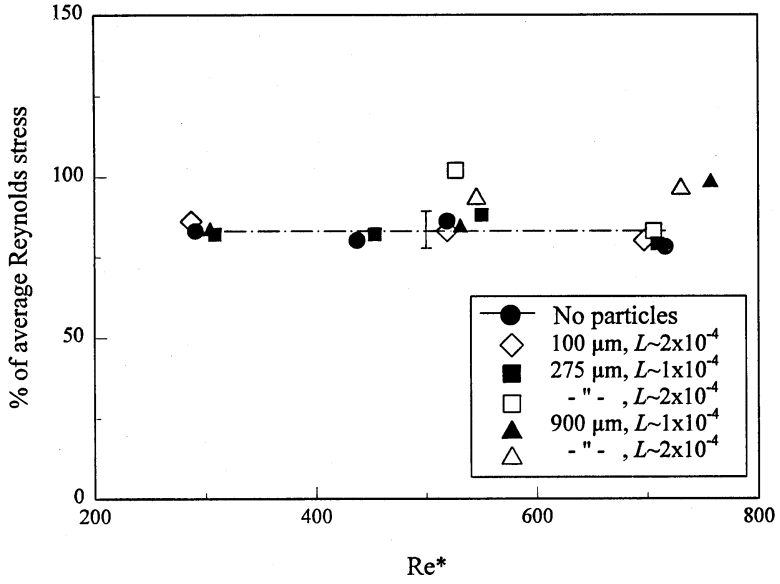

Figure 11. Average portion of Reynolds stress which is contained in the wall structures. Dashed line indicates the average value of all runs without particles. Error bars indicate maximum scatter of particle-free flows.

3.4. *Correlation coefficients*

The effect on the streamwise autocorrelation coefficient by particles is shown in figure 13. The autocorrelation function calculations exhibited relatively large scatter, due to the intermittency of the LDA signal. Therefore the data in the figure were combined such that for each experiment, the correlation coefficient of all the measurements between $y^+ = 30$ and 40 was averaged to produce one data point. As can be seen in the figure, particles generally reduced the autocorrelation coefficient of the flow. Away from the wall the effect of particles on the autocorrelation coefficient diminished. The results in this case are not as distinct as, for example, the modification of the time between structures, but nonetheless the trend is clear. In this sense, the effect

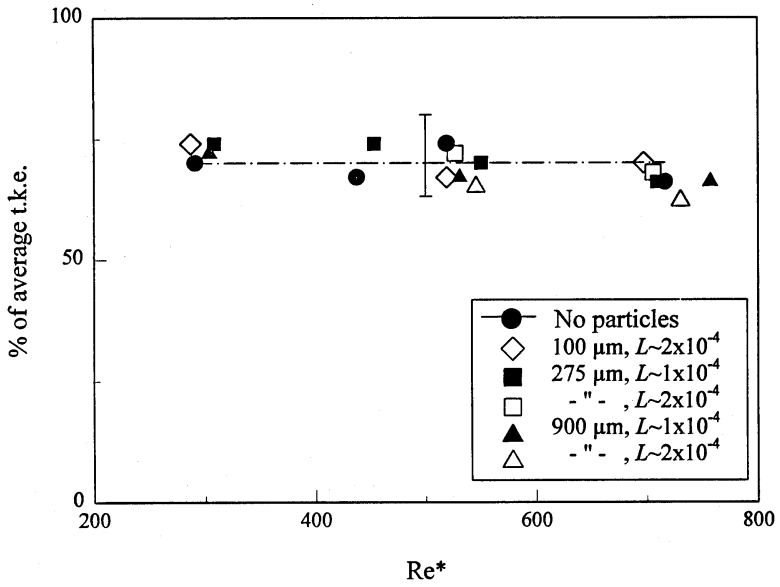

Figure 12. Average portion of turbulent kinetic energy (in 2-D) in funnel vortices. Dashed line indicates the average value of all runs without particles. Error bars indicate maximum scatter of particle-free flows.

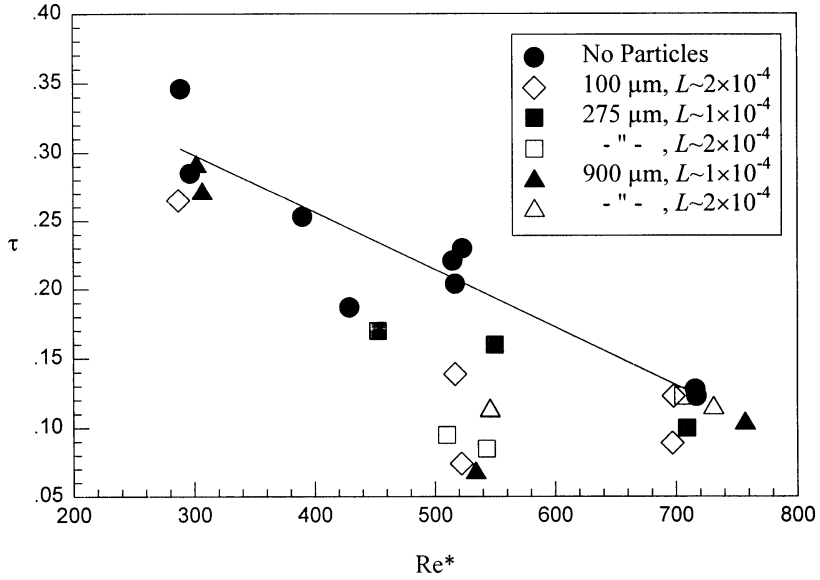

Figure 13. Streamwise autocorrelation coefficients at $y^+ \sim 30$–40. The line is a linear curve fit of no-particles data.

of particles, again, is like that of a rough wall where the longitudinal length scales are shorter than over a smooth wall (Krogstad and Antonia 1994).

3.5. *Quadrant analysis*

Figure 14 depicts the Reynolds stress contributions, of the various quadrants of the u–v plane, to turbulence in the wall region. In general, the second and fourth quadrants are the dominant ones, having the highest contribution to turbulence production, i.e. $-\overline{u'v'}$. These quadrants represent ejections (quadrant II) and sweeps (quadrant IV). With the addition of particles, the Reynolds stress distribution among the quadrants in the wall region changes dramatically. As can be seen in the figure, the relative contribution of quadrant IV increases substantially, a strong motion appears with large particles in quadrant III, and quadrants I and II remain unchanged. The effect is strong very close to the wall and diminishes away from it. The two affected quadrants represent downdrafts of fluid towards the wall, and are probably due to a strong increase in the downflow, or sweep portion of the wall structures.

4. DISCUSSION

It appears that turbulence modulation by particles can occur due to three effects. One is the presence of particles at the wall, where their effect is somewhat similar to stationary roughness elements. Second is the presence and interaction of particles with the wall structures, such as quasi-streamwise vortices, sweeps, and ejections. This appears to be the cause for particle segregation, the modulation of wall structure characteristics, and the enhanced scalar transport rates seen at the wall, which are likely to be the result of the increased wall normal velocity fluctuations. The third effect is the presence and interaction of particles in suspension, away from the wall.

This work was focused primarily on the first two effects. Therefore, the flow conditions were chosen so as to have a large particle concentration close to the wall and a very low concentration of particles in the outer flow. Consequently, effects of particles in suspension could not be noticed here for the most part. For example, turbulence enhancement by large particles due to vortex shedding (see Hetsroni 1989) was not observed. The only situation where particles affected the turbulence due to the third effect in this work was at the high Reynolds number flows with small particles, where many particles were suspended. There the Reynolds stress was

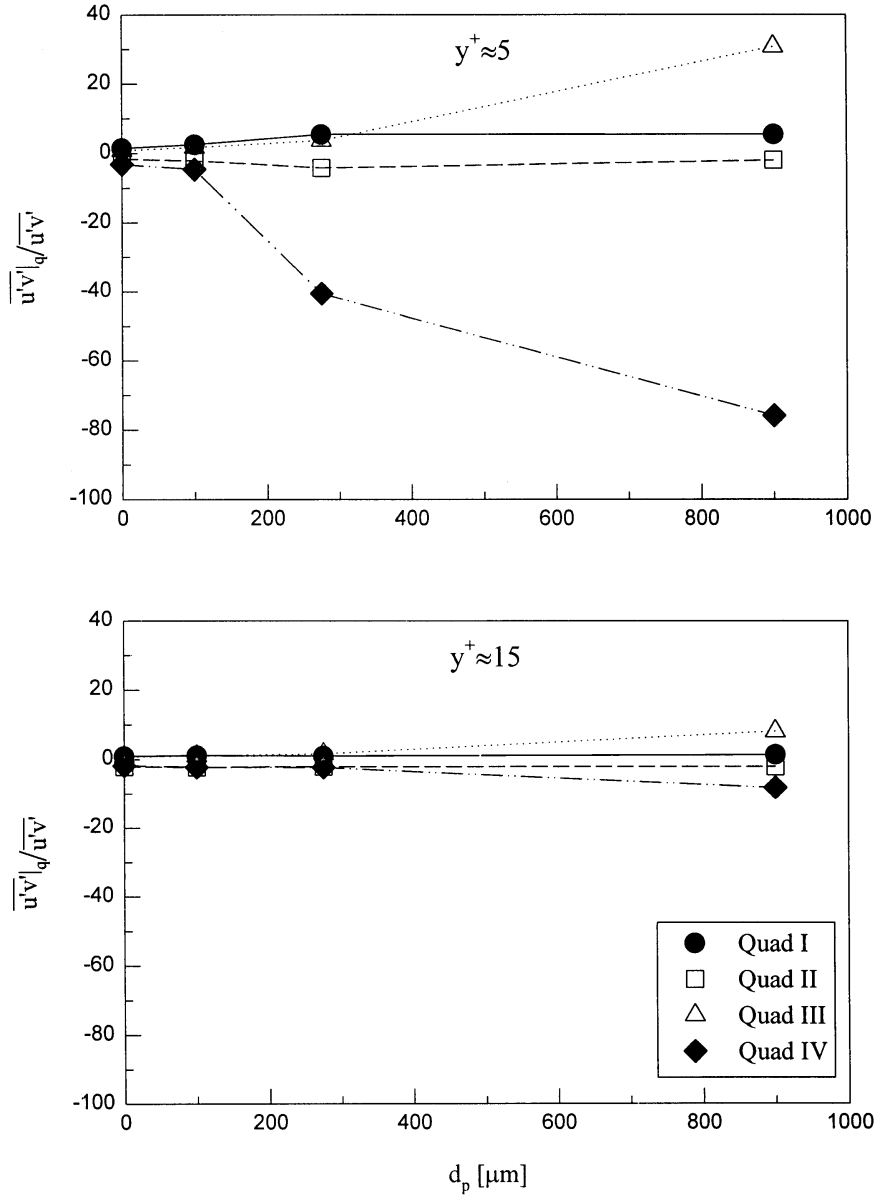

Figure 14. Relative contributions to Reynolds stress by quadrants. Top: $y^+ = 5$; bottom: $y^+ = 15$.

somewhat suppressed – in agreement with the findings of other researchers (e.g. Tsuji and Morikawa, 1982; Hetsroni, 1989).

The rough wall effects observed here were small, and consisted primarily of an increase of the wall shear stress, a reduction of the mean velocity and an increase in turbulence production. The fact that the effects seem to be relatively small is not surprising, considering that the non-dimensional equivalent sand roughness was within the hydraulically smooth regime ($k_s^+ < 5$). In addition, since the particles tend to concentrate in the low-speed regions, where the local shear rate is small, their influence was probably even less significant.

It should be remembered that the values of k_s^+ were evaluated here from the deviation of the velocity profiles from those of particle-free flow. In other words, the equivalent sand roughness is a measure of the effect of the particles. The mechanism of how those effects are brought about is yet to be determined, and it does not indicate that particles affect the flow in the same way as roughness elements of equivalent sizes.

The concentration of particles in suspension, away from the wall, was, in most of these cases, quite small. Therefore, turbulence production by particles in this region was negligible.

The fact that only some of the modulations of turbulence can be attributed to a roughness effect is important because it implies the significance of the second effect above. The presence of particles at the wall, together with their interaction with the wall structures, caused a reduction in the frequency of occurrence of these structures. The reduction seems to scale with the second power of the non-dimensional particle size, as shown in figure 10. These data suggest that the reduction in frequency should, in fact, scale with the non-dimensional particle relaxation time, as well as size. Experiments with other particle densities must be performed to examine this point. Nonetheless, it seems that the frequency is directly related to particle size and to wall variables.

In spite of the notable reduction in the number of structures, the relative amount of Reynolds stress and turbulent kinetic energy contained in them did not change significantly (figures 11 and 12). This is probably because the structures that do evolve, in spite of the presence of particles, are more energetic than those in particle-free flow. This hypothesis was recently substantiated by Niño and Garcia (1996). It is also supported here by the reduction in the streamwise autocorrelation coefficient (figure 13), which suggests that the structures are more 'intense'. The added intensity seems to be concentrated in the sweep events which increased significantly relative to particle-free flow. It is also possible that in the presence of particles the structures persist for longer periods of time, which would also enhance their relative share in turbulence production.

The observed turbulence modulations at the wall may serve to clarify how particles affect transport rates at the wall. Campbell and Hanratty (1983) derived an approximate expression for the average mass transfer coefficient at the wall for relatively high Schmidt numbers as:

$$\bar{K} \sim \mathrm{S}^{-0.7}(\overline{\beta^2})^{0.21} \qquad [4]$$

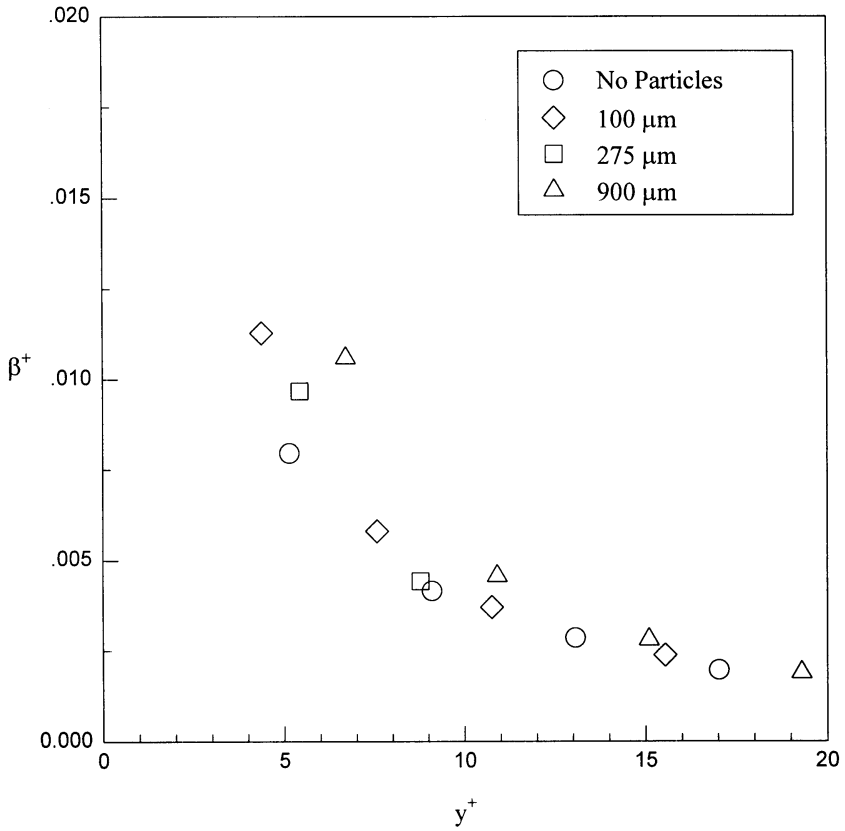

Figure 15. Mean non-dimensional velocity fluctuations parameter in the vicinity of the wall at $Re_h \approx 10{,}000$. The data were corrected for Doppler frequency broadening due to the strong velocity gradient inside the measuring volume (Edwards *et al.* 1971), and assuming no correlation between the velocity fluctuations and frequency broadening.

where S is the Schmidt number and β is an approximation for the wall normal velocity fluctuations, given by

$$v' = \beta(x,z,t)y^2. \quad [5]$$

Thus knowledge of the wall normal r.m.s. in the wall region can be applied in making rough estimates of the mass transfer coefficient. [4] can also be used for evaluating heat transfer rates by replacing K and S by a heat transfer coefficient and Prandtl number, respectively.

Values of β at $Re_h \sim 10{,}000$, normalized by wall units, are plotted in figure 15. Without particles, the values are close to other experimental values found in the literature (see Finnicum and Hanratty 1985). With particles, values of β increase, giving higher values for larger particles. A similar result was found in simulations by Pan and Banerjee (1996). This behavior is consistent with the observed enhancement of heat transfer rates in particle-laden flows. Unfortunately, it is not possible to accurately determine a value of β right at the wall because of uncertainties in the measurements of v' there, e.g. due to increased noise when the LDA measuring volume touches the wall. However, it is possible to roughly estimate the increase in transfer rates based on the ratios of β for particle-free and particle-laden flows some distance from the wall. For example, in figure 15, with the 900 μm particles, the difference is of the order of 25%, thus predicting a 18% increase in transfer rate (when the friction velocity of particle-free flow is used). This value is close to the enhancement of heat transfer with particles, under similar conditions, in the work of Hetsroni and Rozenblit (1994). They found an increase of approximately 20% at $Re_h \approx 5000$.

5. CONCLUDING REMARKS

In summary, the presence of particles in large concentrations near the wall affects turbulence in the boundary layer in two ways. One is an effect similar to a rough wall, and the other is by interaction with the turbulence structures. Since particles tend to accumulate in the low-speed regions, they increase the apparent roughness there, resulting in a localized increase of the heat transfer coefficient. Since the wall shear stress in these regions is initially low, compared to the high-speed regions, the increased roughness does not adversely affect the wall friction and overall pressure drop.

The particles also reduce the number of wall structures per unit time, compared with flow without particles. The reduction is proportional to the particle size and concentration at the wall. However, it appears that the structures that do develop are more energetic, compared to particle-free flow, particularly in the sweep portion. Therefore, the relative contribution of the structures to the Reynolds stress and turbulent kinetic energy are essentially unchanged.

Acknowledgements—We would like to express our gratitude to the Electric Power Research Institute for support of this project under Grant No. DE-FG3-85ER13314, and to the National Science Foundation, Grant No. CTS88-22056.

REFERENCES

Achenbach, E. (1974) Vortex shedding from spheres. *J. Fluid Mech.* **62,** 209–221.

Bernard, P. S., Thomas, J. M. and Handler, R. A. (1993) Vortex dynamics and the production of Reynolds stress. *J. Fluid Mech.* **253,** 385–419.

Brooke, W., Kontomaris, K., Hanratty, T. J. and McLaughlin, J. B. (1992) Turbulent deposition and trapping of aerosols at a wall. *Phys. Fluids A* **4,** 825–834.

Brooke, J. W. and Hanratty, T. J. (1993) Origin of turbulence-producing eddies in a channel flow. *Phys. Fluids A* **5,** 1011–1022.

Campbell, J. A. and Hanratty, T. J. (1983) Mechanism of turbulent mass transfer at a solid boundary. *AIChE J.* **29,** 221–229.

Edwards, R. V., Angus, J. C., French, M. J. and Dunning, J. W. Jr. (1971) Spectral analysis of the signal from the laser Doppler flowmeter: time-independent systems. *J. Appl. Phys.* **42,** 837–850.

Finnicum, D. S. and Hanratty, T. J. (1985) Turbulent normal velocity fluctuations close to a wall. *Phys. Fluids* **28,** 1654–1657.

Gore, R. and Crowe, C. T. (1989) Effect of particle size on modulating turbulent intensity. *Int. J. Multiphase Flow* **15,** 279–285.

Grass, A. J. (1982) The influence of boundary layer turbulence on the mechanics of sediment transport. In *Euromech 156: Mechanics of Sediment Transport*, Istanbul, p. 3.

Grass, A. J., Stuart, R. J. and Mansour-Tehrani, M. (1991) Vortical structures and coherent motion in turbulent flow over smooth and rough boundaries. *Philos. Trans. Roy. Soc. London A* **336,** 35–65.

Hetsroni, G. (1989) Particle–turbulence interaction. *Int. J. Multiphase Flow* **15,** 735–746.

Hetsroni, G. and Rozenblit, R. (1994) Heat transfer to a liquid solid mixture in a flume. *Int. J. Multiphase Flow* **20,** 671–689.

Hinze, J. O. (1975) *Turbulence*, 2nd edn. McGraw-Hill, New York.

Ishii, M. (1977) One-dimensional drift-flux model and constitutive equations for relative motion between phases in various two-phase regimes. Report ANL-77-47, Argonne National Laboratory, Argonne, IL.

Kaftori, D. (1993) Structures in the turbulent boundary layer and their interaction with particles. Ph.D. Dissertation, University of California at Santa Barbara.

Kaftori, D., Hetsroni, G. and Banerjee, S. (1994) Funnel-shaped vortical structures in wall turbulence. *Phys. Fluids* **6,** 3035–3050.

Kaftori, D., Hetsroni, G. and Banerjee, S. (1995a) Particle behavior in the turbulent boundary layer. Part I: Motion, deposition, and entrainment. *Phys. Fluids* **7,** 1095–1106.

Kaftori, D., Hetsroni, G. and Banerjee, S. (1995b) Particle behavior in the turbulent boundary layer. Part II: Velocity and distribution profiles. *Phys. Fluids* **7,** 1007–1121.

Krogstad, P.-A. and Antonia, R. A. (1994) Structure of turbulent boundary layers on smooth and rough walls. *J. Fluid Mech.* **277,** 1–21.

Lam, K. and Banerjee, S. (1992) On the conditions of streak formation in a bounded turbulent flow. *Phys. Fluids A* **4,** 306–320.

Lázaro, B. J. and Lasheras, J. C. (1989) Particle dispersion in a turbulent, plane, free shear layer. *Phys. Fluids A* **1,** 1035–1044.

Lee, S. L. and Börner, T. (1987) Fluid flow structure in a dilute turbulent two-phase suspension flow in a vertical pipe. *Int. J. Multiphase Flow* **13,** 233–246.

Leighton, D. and Acrivos, A. (1986) Viscous resuspension. *Chem. Eng. Sci.* **41,** 1377–1384.

Luchik, T. S. and Tiederman, W. G. (1987) Timescale and structure of ejections and bursts in turbulent channel flows. *J. Fluid Mech.* **174,** 529–552.

Mei, R., Adrian, R. J. and Hanratty, T. J. (1991) Particle dispersion in isotropic turbulence under Stokes drag and Basset force with gravitational settling. *J. Fluid Mech.* **225,** 481–495.

Nezu, I. and Rodi, W. (1986) Open-channel flow measurements with a laser Doppler anemometer. *J. Hydraulic Eng.* **112,** 335–355.

Niño, Y. and Garcia, M. H. (1996) Experiments on particle–turbulence interactions in the near-wall region of an open channel flow: implications for sediment transport. *J. Fluid Mech.* **326,** 285–319.

Pan, Y. and Banerjee, S. (1996) Numerical simulation of particle interaction with wall turbulence. *Phys. Fluids* **8,** 2733–2755.

Pedinotti, S., Mariotti, G. and Banerjee, S. (1993) Direct numerical simulation of particle behaviour in the wall region of turbulent flows in horizontal channels. *Int. J. Multiphase Flow* **18,** 927–941.

Rashidi, M. and Banerjee, S. (1988) Turbulence structure in free-surface channel flows. *Phys. Fluids* **31,** 2491–2503.

Rashidi, M. and Banerjee, S. (1990) The effect of boundary conditions and shear rate on streak formation and breakdown in turbulent channel flow. *Phys. Fluids A* **2,** 1827–1838.

Rashidi, M., Hetsroni, G. and Banerjee, S. (1990) Particle–turbulence interaction in a boundary layer. *Int. J. Multiphase Flow* **16,** 935–949.
Robinson, S. K. (1991) Coherent motions in the turbulent boundary layer. *Ann. Rev. Fluid Mech.* **23,** 601–639.
Schlichting, H. (1979) *Boundary Layer Theory*, 7th edn. McGraw-Hill, New York.
Shuen, J.-S., Solomon, A. S. P., Zhang, Q.-F. and Faeth, G. M. (1985) Structure of particle-laden jets: measurements and predictions. *AIAA J.* **23,** 396–404.
Smith, J. D. and McLean, S. R. (1977) Spatially averaged flow over a wavy surface. *J. Geophys. Res.* **82,** 1735–1746.
Squires, K. D. and Eaton, J. K. (1991) Preferential concentration of particles by turbulence. *Phys. Fluids A* **3,** 1169–1178.
Sumer, B. M. and Oguz, B. (1978) Particle motion near the bottom in turbulent flow in an open channel. *J. Fluid Mech.* **86,** 109–127.
Sun, T.-Y. and Faeth, G. M. (1986) Structure of turbulent bubbly jets – I. Methods and centerline properties. *Int. J. Multiphase Flow* **12,** 99–114.
Talmon, A. M., Kunen, J. M. G. and Ooms, G. (1986) Simultaneous flow visualization and Reynolds-stress measurement in a turbulent boundary layer. *J. Fluid Mech.* **163,** 459–478.
Tsuji, Y. and Morikawa, Y. (1982) LDV measurements of an air–solid two-phase flow in a horizontal pipe. *J. Fluid Mech.* **120,** 385–409.
Tsuji, Y., Morikawa, Y. and Shiomi, H. (1984) LDV measurements of an air–solid two-phase flow in a vertical pipe. *J. Fluid Mech.* **139,** 417–434.
Wang, L. P. and Maxey, M. R. (1993) Settling velocity and concentration distribution of heavy particles in homogeneous isotropic turbulence. *J. Fluid Mech.* **256,** 27.
Yung, B. P. K., Merry, H. and Bott, T. R. (1989) The role of turbulent bursts in particle re-entrainment in aqueous systems. *Chem. Eng. Sci.* **44,** 873–882.
Zisselmar, R. and Molerus, O. (1979) Investigation of solid–liquid pipe flow with regard to turbulence modification. *Chem. Eng. J.* **18,** 233–239.

APPENDIX A

Identification Of Flow Structures In LDA Data

While structural features of turbulence may be apparent in various flow visualization techniques, they are not clearly evident in point measurements. Obtaining information regarding these structures from a stream of data requires conditional sampling, where a flow structure is said to occur if some conditions, relating to some detection function, are fulfilled (see Luchik and Tiederman, 1987 for a review of some conditional sampling methods). The major drawback of available techniques is their reliance on factors such as threshold levels and a grouping window, as discussed below. These factors are not readily available. Although some methods for obtaining these factors have been suggested (e.g. Luchik and Tiederman, 1987), they are not free of subjective estimates on the one hand, or relying on flow visualization on the other, and are, therefore, not completely general.

In this work, flow structures were detected in the LDA data as events (i.e. 'active' periods) by a combination of the $u'v'$ and ***tke*** techniques. In this method an event is said to occur if either the instantaneous Reynolds stress or the turbulent kinetic energy exceed some threshold level. These events are then put together into groups representing wall structures. The necessary parameters, namely the threshold levels for detection and the time window for grouping, are found through an iterative optimization process using an objective algorithm. The technique was developed and tested with the aid of simultaneous flow visualization using high-speed video.

Observations Of Flow And Data

Figure 16 depicts the instantaneous values of Reynolds stress and the two dimensional turbulent kinetic energy of a portion of a typical data file at $\mathrm{Re}_h \approx 5000$ and $y^+ \approx 30$. The two quantities are normalized by the relation

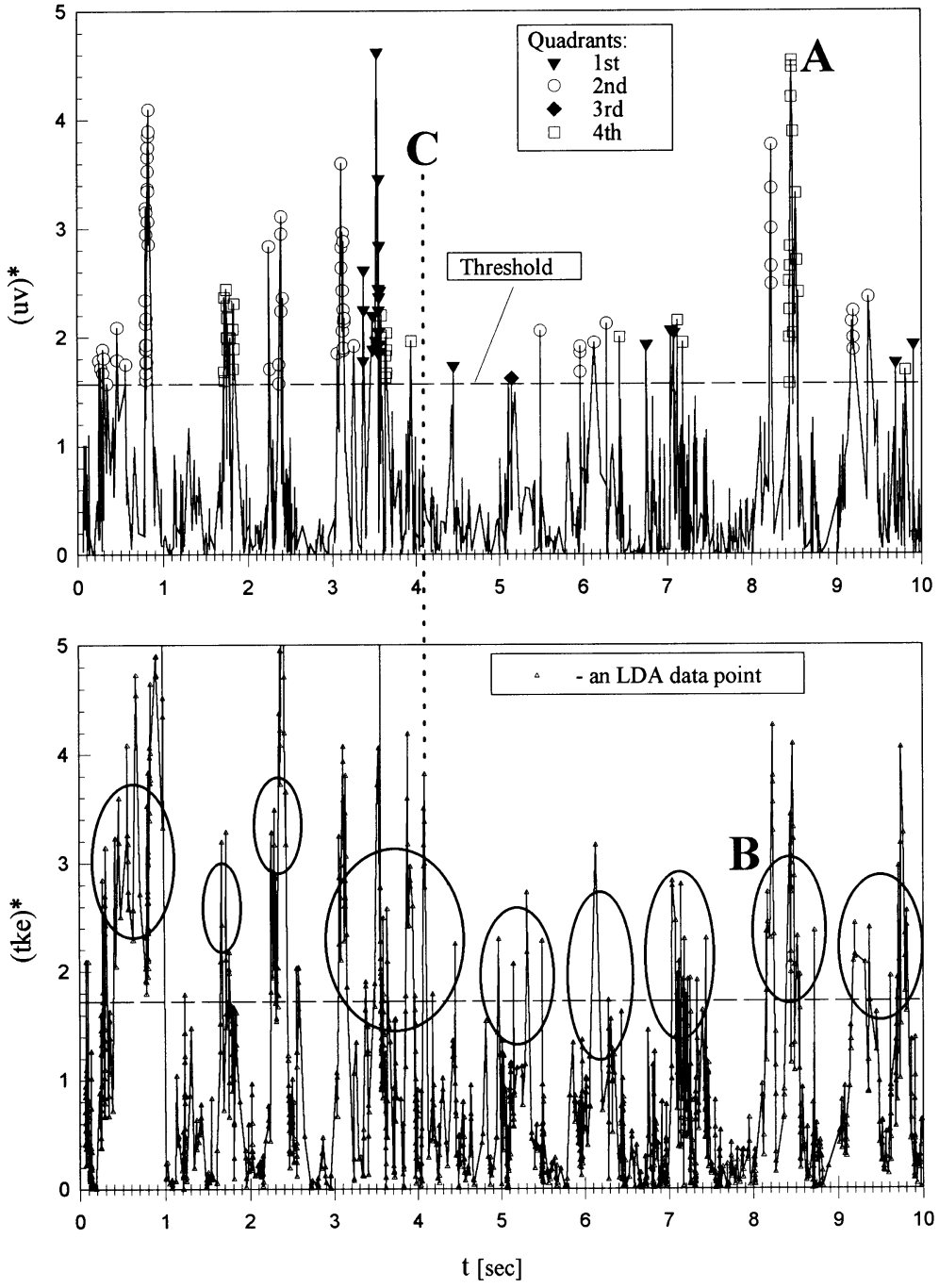

Figure 16. Instantaneous normalized Reynolds stress (top) and two dimensions of turbulent kinetic energy (bottom) of a typical LDA file. Circles designate groups of events which correspond to wall structures. $Re_h = 5000$. $y^+ \approx 30$. (A) Multiple events where only a single flow structure occurred. (B) A wall structure containing three events. (C) An event showing as a *tke* peak only.

$$uv^* = \left| \frac{u'v'}{uv} \right|$$

$$tke^* = \frac{u'2 + v'2}{u^2 + v^2} \qquad [A1]$$

where primes denote the fluctuating velocity components in the Reynolds decomposition and

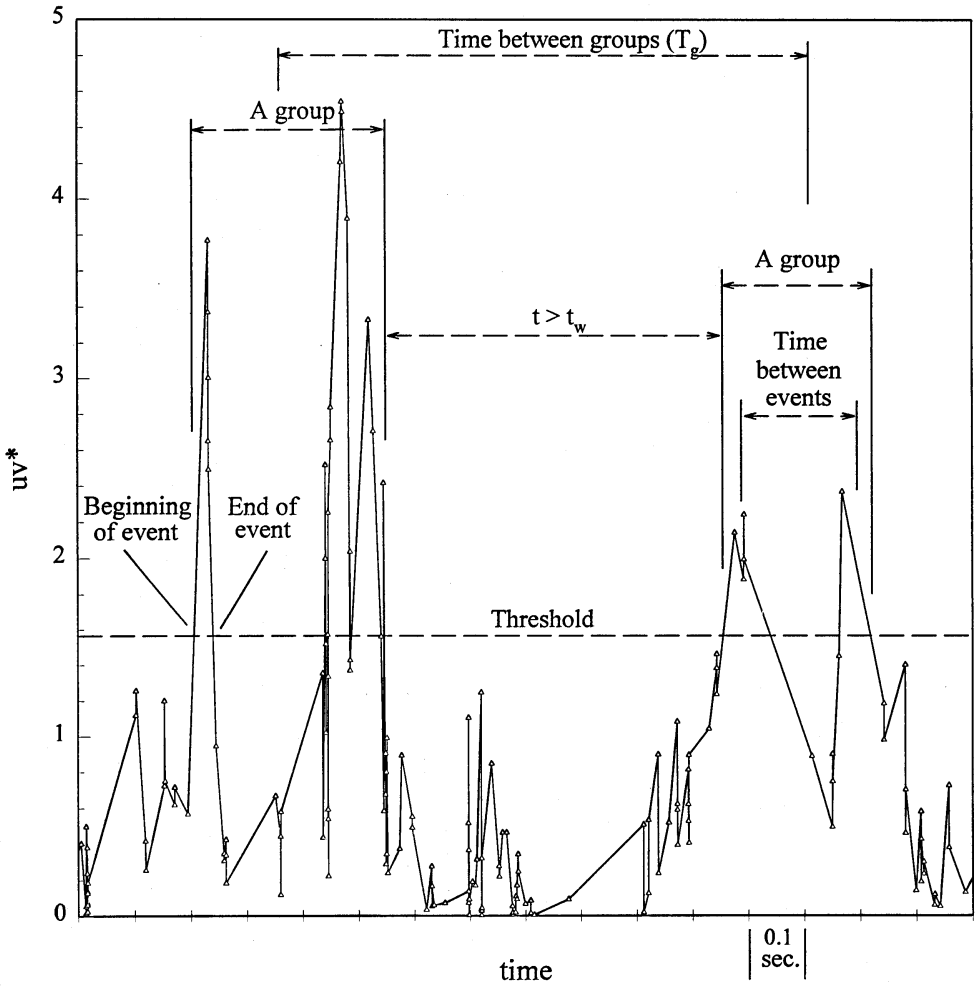

Figure 17. Illustration of the definition of terms.

symbols without a prime are r.m.s. values (e.g. $u = \sqrt{\overline{u'2}}$). This type of normalization was used because it yields consistent and comparable values under various flow conditions for both the Reynolds stress and kinetic energy. The data in the figure contain distinct portions of high ***uv**** and ***tke****, and in general the peaks of ***uv**** and ***tke**** coincide in time. Observations of high speed videos, synchronized with such plots of LDA data, show that the peaks and the flow structures are related as follows.

- The sets of peaks of *uv** and/or *tke** are characteristics of wall structures, consisting of ejections and sweeps. For clarity of presentation, peaks whose levels of either *uv** or *tke** are greater than some predetermined thresholds will henceforth be referred to as events. The choice of threshold will be discussed later. A definition of an event, together with other terms discussed here, is illustrated in figure 17, which is an enlarged portion of figure 16.
- There are three distinct frequencies in the data. First is the frequency associated with events which are multiple detections of the same internal structure. Here an 'internal' structure is a flow pattern that is part of a larger structure, such as one ejection within a burst (where a burst often comprises a number of ejections). An example of this frequency is denoted by A in figure 16, where there are a few closely spaced peaks, but where only a single long sweep was apparent on video. The second frequency is that of appearance of internal structures, such as separate ejections inside one burst. For example, in the structure denoted by B in figure 16, which was composed of three events. The third is that of the wall structures themselves. The first frequency does not represent a physical quantity. It is an artifact of the measuring technique and data acquisition rate, and has also been noted by Talmon *et al.*

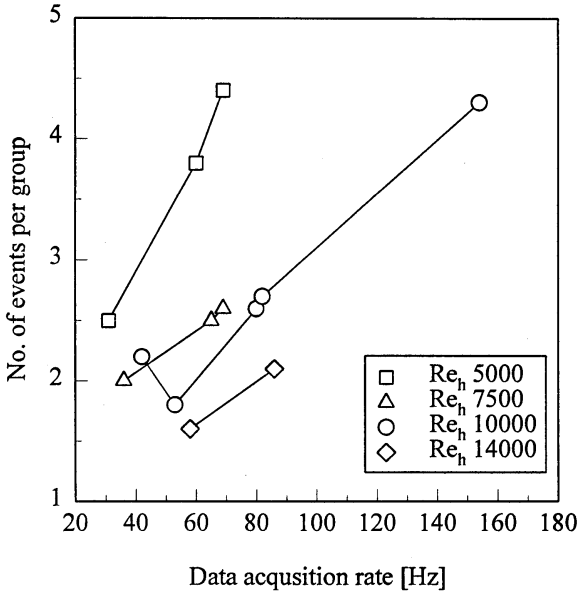

Figure 18. Average number of events in groups vs. LDA data rate.

(1986) and by Luchik and Tiederman (1987). The first and second frequencies are often close to one another, especially at higher Reynolds numbers, where the second frequency becomes high and tends to overlap the first one. These relationships can be deduced from figure 18, where it can be seen that fewer events are detected in structures at higher Reynolds numbers, and that the number of detections increases with increasing data rate.

• In most cases, an event is apparent as both *uv** and *tke** peaks. However, there are cases where only one of the two can be seen, as illustrated by C in figure 16. Therefore, it is best to utilize both parameters when scanning for events.

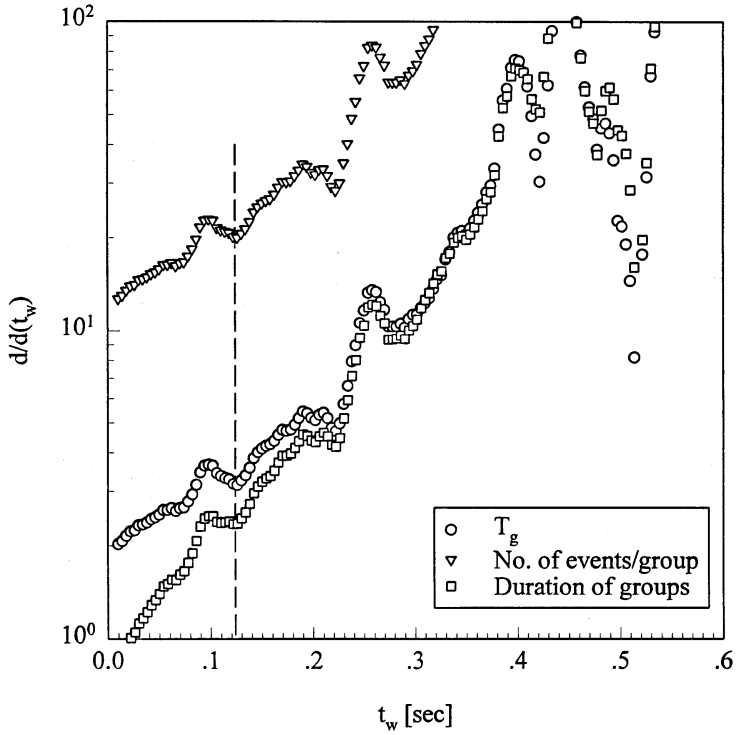

Figure 19. Local derivatives of average group characteristics vs. grouping window. The best grouping window for the given threshold is approximately 0.125 s.

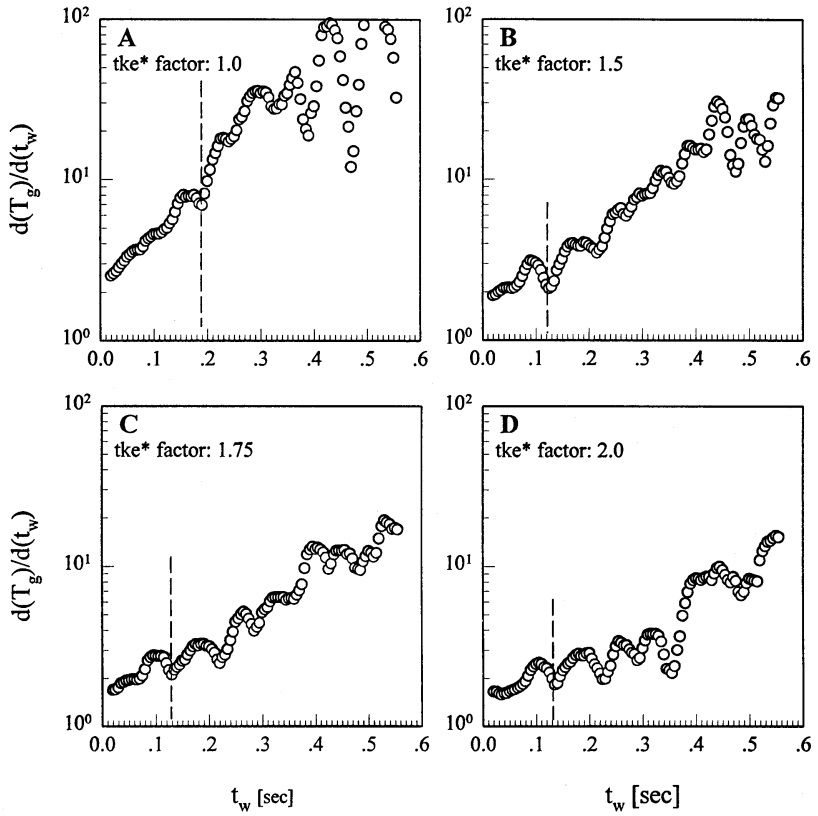

Figure 20. Variation of grouping window with *tke* threshold factor.

- The type of events, namely ejections or sweeps, can be identified by the quadrant of the product $u'v'$ in the u'–v' plane (figure 16). Occasionally, however, a sample within an event may be of a different quadrant than the other samples due to random noise and turbulence. The data in the figure, and in all subsequent analysis, was treated so that each event was designated as belonging to the quadrant which contained the majority of the samples. Comparison of plots produced in such a way, with video, shows good agreement.

- A wall structure is generally made of a group of events. These groups stand out above the 'noise' level in the data, and as seen in figure 16, are spaced rather uniformly apart. In order to identify the individual structures, one must combine the events that belong to each group, as discussed below (see also figure 17). Many structures consist of combinations of events of various types, the majority of which are ejections (quadrant 2 in the u'–v' plane), and sweeps (quadrant 4). A small number of events from the first and third quadrant also appear.

Grouping Algorithm

Three parameters must be determined for identification and grouping of events into groups representing flow structures. These are the two threshold values (for uv^* and tke^*), and the time window for grouping. The grouping window is a time frame which is larger than the average time between events but is shorter than the average time between groups. In the detection process, the time between each two consecutive events is compared to the grouping window. If it is shorter than the grouping window, then the events are said to belong to the same group. If the time between events is longer than the grouping window, the events are said to belong to separate groups. Ideally, the time between events would be much shorter than the average time between bursts. If this was true, then it would have been easy to distinguish between the two.

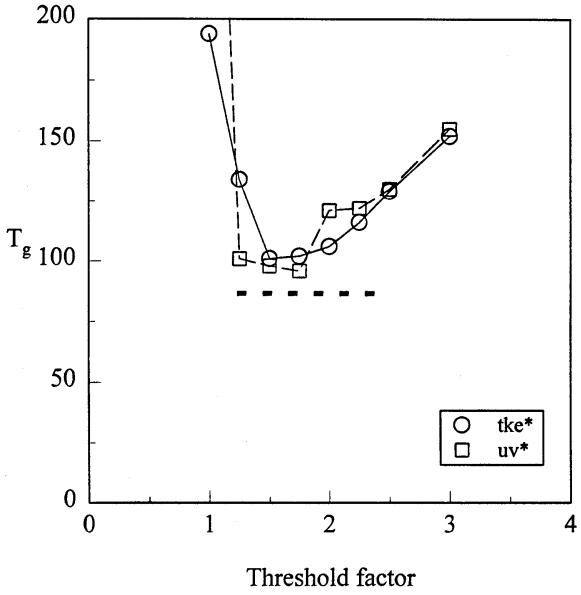

Figure 21. Variation of T_g, computed with t_w found using figure 20, with threshold factors. The horizontal dashed line shows T_g which is found when both the $u'v'$ and *tke* techniques are used.

Unfortunately, this is not usually the case because the actual distribution of times in the data overlap and a clear distinction is difficult to make (see also Luchik and Tiederman 1987).

The technique of finding the best thresholds and grouping window is a systematic optimization process where all three values are searched for simultaneously. The basic premise is that when the correct grouping window and threshold levels are found, there will be a point where a small change of the detection parameters in a given experiment will not have a significant impact on the characteristics of the groups, such as the average time between them. In other words, when the average normalized time between groups is plotted against the grouping window, there will be a region with only a small gradient in the curve. More noticeably, there will be a minimum of the first derivative in that region. In fact, there should be a minimum corresponding to each of the three frequencies described above, but as will be seen shortly, only the second and third frequencies can usually be identified clearly.

Grouping Window

This idea is illustrated in figure 19 where the local derivative, $\mathrm{d}(T_g)/\mathrm{d}(t_w)$, of the discrete function $T_g(t_w)$, is plotted against t_w for some threshold levels of uv^* and tke^*. Here t_w is the grouping window and T_g is the average time between groups, normalized by inner variables:

$$T_g = \frac{u^{*2}}{\nu} t_g \qquad [A2]$$

where t_g is the dimensional average time between groups. Also plotted are the local derivatives of the average duration of groups, and the average number of events per group. The local derivatives $\mathrm{d}/\mathrm{d}(t_w)$ in this analysis were determined by fitting a first order polynomial through the points of $T_g(t_w)$ in the vicinity of t_w, and differentiating analytically.

As can be seen in figure 19, there appear distinct minima in the curves [i.e. $\mathrm{d}^2/\mathrm{d}(t_w)^2 = 0$]. In general, the minima of the various quantities coincide. For the given (and at this point still arbitrary) threshold level in the figure, the distinct minimum that corresponds to the lowest grouping window is the best one. Here the best minimum will be denoted t_b and in figure 19 it is at $t_b \approx 0.125$ s. The best minimum is the one corresponding to the correct grouping window (t_w). However, thus far this is true only for the given (and as yet arbitrary) threshold. The selection of the best t_w for the whole experimental run must be determined together with the correct threshold levels, as discussed next.

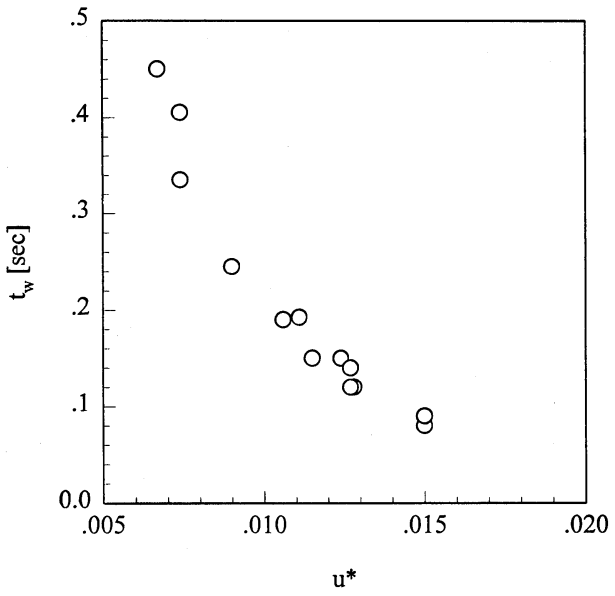

Figure 22. Variation of grouping window with friction velocity.

Threshold Levels

In selecting the best threshold levels and grouping window, it is convenient to present the thresholds in terms of threshold factors f_{tke} and f_{uv}, which may be defined by:

$$tke \text{ threshold} = f_{tke} \times \overline{tke^*}$$

$$uv \text{ threshold} = f_{uv} \times \overline{uv^*} \qquad [A3]$$

where an overbar indicates an integrated mean of the whole experimental run.

The selection of these factors, together with t_w, is a two stage iterative process. In the first stage a separate plot of $d(T_g)/d(t_w)$, similar to figure 19, is plotted for a number of threshold levels. This is shown in figure 20. Next, a best grouping window is established for each threshold level (shown by vertical dashed lines in the figure). Tracing the trend in figure 20, one can see that at a low threshold the first minimum (t_b) is relatively high. It then becomes lower as the threshold is raised. When the threshold is raised further, the location of t_b becomes relatively constant. At this time, a new local minimum, at a lower value of t_w, may appear [$t_w \sim 0.04$ s in figure 20(D)]. This minimum corresponds to the average time between events in the data, and will be referred to as t_e. Note that indications of this minimum begin to appear at lower thresholds (i.e. a bend in the curve).

In the second stage of the process, the average time between groups is calculated for each threshold using the corresponding t_b. The variations of T_g are then plotted against the threshold levels as in figure 21. At low threshold levels many peaks, which correspond to noise and random fluctuations, are detected. Consequently there is no distinct separation between groups and the average time between groups is long. At higher threshold levels less of the noise is captured and the true time between groups becomes evident. At still higher thresholds, the lower peaks, which correspond to weaker structures, do not clear the threshold and the average time between groups increases. Therefore, the threshold level which corresponds to the lowest T_g is the best one. This process should be done twice, once in search of f_{tke}, where *uv* is not considered ($f_{uv} \rightarrow \infty$), and again in search of f_{uv}, where *tke* is not considered (figure 21).

The final step in the process is to re-plot $d(T_g)/d(t_w)$ with both *tke* and *uv* active, each with its own threshold factor, and to establish the best t_w and then T_g for the combined technique. These are the best values of the particular experiment.

Application Of The Algorithm

Applying this procedure to the run used in the illustrations, we see from figure 21 that the best threshold factors are 1.5 for *tke* and 1.75 for *uv*. The grouping windows for *tke* in the plot were taken from figure 20 (the corresponding plot for threshold levels of *uv* is not shown). These threshold values were combined to produce figure 19, where the best t_w is 0.125 s. The average time between groups, using these thresholds and grouping window, was 92.1 which is indicated by the dotted line in figure 21.

The advantage of using the combined, rather than only the $u'v'$ or *tke* techniques is evident in figure 21. Each method, when used separately, yields a higher T_g than the combined technique. This is a typical result indicating that some groups which may be missed by one technique are captured by the other. Neither one of the two by itself is sufficient.

Finally, one additional situation required special treatment in the analysis. It became evident, by comparison of LDA data and visualization, that occasionally there appeared active 'long' periods which did not qualify as ejections or sweeps. From visualization it was determined that such periods often occurred as an extension of a structure, which usually ended at the next structure. Alternatively, there may, on occasion, have been a streamwise vortex whose axis was located in front or past the plane of view and did not pass directly through the measuring point. In the data these periods appeared as long sequences of *uv** or *tke** of various quadrants, most of which were only slightly higher than the threshold level. An example of such a situation is in the region between 5 and 7.2 s of the *uv** plot in figure 16.

In order to detect the structures which may be hidden in the long active periods, one more step was added to the detection algorithm. First the 'long groups' were identified by virtue of their length since they were typically about three times longer than the average duration of groups. Next these structures were re-scanned for events within them but with the threshold factors raised by one unit. If a long group could be split into two (or more) new ones with the higher threshold, then the new groups replaced the original one. In the example above, the long region between 5 and 7.2 s of the plot in figure 16 was split into three separate groups. If the long group could not be split, then it remained as a single structure and nothing was changed. This procedure was done routinely as part of the optimization process. Typical, about 10% of the originally-detected groups were long, of which nearly 50% could be split using the algorithm above. When this procedure was used, the average time between groups was of the order of 5% lower than without it.

Evaluation Of The Technique

The combined *uv* and *tke* technique was evaluated by comparison with synchronized visualization of microbubble tracers and other available data. For example, the results obtained, such as the time between bursts, were compared with values in the literature.

In general, the various parameters involved in the technique were consistent and independent of experimental and flow conditions. For example, the threshold factors were independent of data rate or Reynolds number. The average threshold factor for *tke* was 1.75–2 while for *uv* it was approximately 2.25. One should note, however, that the actual threshold is approximately twice the mean *uv** and *tke** in both cases, and that the difference in threshold factors stems from the different definitions of *uv** and *tke**, the former being a mean of a product while the latter is a mean of a sum of products (see [A1]). These values are in agreement with the conclusion of Talmon *et al.* (1986) who found, based on visualization, that the best threshold level was twice the mean *uv*.

The grouping window, on the other hand, does exhibit an inverse dependence on flow conditions, as illustrated in figure 22. This is expected since as the friction velocity increases, the time scale of the occurrence of the structures decreases.

Comparisons of the technique to flow visualization at $Re_h \approx 5000$ show that practically all of the wall structures which were observed on video were also detected in the LDA data. However, not all detections were one to one. For example, in some cases a burst in visualization was

detected as two in the data because a longer than average time elapsed between separate events. Other times this happened because one of the internal structures, or portions of it, which could be seen on video did not produce high levels of uv^* or tke^* and were not recognized. During these undetected events there was a long pause in the middle of the group in the data, which caused it to be mis-identified as two separate groups. These cases of mis-identification were balanced by cases where what appeared as two separate structures on video was detected as a single one in the data because the time between them was shorter than the grouping window. In addition in approximately 5% of the cases, bursts were detected in the data while no special activity could be seen on video. In all, some type of mis-identification occurred in about 25% of the cases but, as mentioned above, many of the occurrences caused opposite effects, thus balancing each other. Overall, the number of groups detected in the data was $\pm 5\%$ of the number of structures observed in flow visualization.

Finally, it should be noted that the presence of particles did not alter any of the parameters of the technique. The only exception was the grouping window which was increased by approximately 25% with large particles. This is not surprising in view of the fact that particles reduce the frequency of appearance of the structures.